Structure and $2p$ decay mechanism of ^{18}Mg[*]

L. Zhou (周龙),[1,2] D. Q. Fang (方德清) ,[1,2,†] S. M. Wang (王思敏) ,[1,2,‡] and H. Hua (华辉)[3]

[1]*Key Laboratory of Nuclear Physics and Ion-beam Application (MOE),*
Institute of Modern Physics, Fudan University, Shanghai 200433, China
[2]*Shanghai Research Center for Theoretical Nuclear Physics,*
NSFC and Fudan University, Shanghai 200438, China
[3]*School of Physics and State Key Laboratory of Nuclear Physics and Technology, Peking University, Beijing 100871, China*

The recently discovered, extremely proton-rich nuclide ^{18}Mg exhibits ground-state decay via two sequential two-proton ($2p$) emissions through the intermediate nucleus, ^{16}Ne. This study investigates the structure and the initial $2p$ decay mechanism of ^{18}Mg by examining the density and correlations of the valence protons using a three-body Gamow-coupled-channel method. The results show that the ground state of ^{18}Mg is significantly influenced by the continuum, resulting in a significant s-wave component. However, based on the current framework, this does not lead to a significant deviation in mirror symmetry in either the structure or spectroscopy of the ^{18}Mg-^{18}C pair. Additionally, the time evolution analysis of the ^{18}Mg ground state suggests a simultaneous $2p$ emission during the first step of decay. The observed nucleon–nucleon correlations align with those of the light–mass $2p$ emitters, indicating a consistent decay behavior within this nuclear region.

Keywords: Structure of ^{18}Mg, two-proton decay, proton–proton correlation

I. Introduction

In recent decades, remarkable advancements have been made in extending the boundaries of nuclear stability, leading to the discovery of numerous dripline nuclides. These nuclides, which are characterized by a significant imbalance in their proton–neutron ratios, exhibit exotic modes of radioactivity and are significantly influenced by the continuum effect. Notably, two-proton ($2p$) emission, initially proposed by Goldansky in the early 1960s [1, 2], has only been observed in recent years [3, 4], making it a particularly rare form of radioactivity. This decay process is essentially a three-body quantum-tunneling phenomenon occurring in extremely proton-rich nuclei. It indicates the complex interplay between the daughter nucleus and valence protons [5–9]. The decay mechanisms vary across different 2p emitters [10–14], encompassing diproton decay and large-angle emission [15–18], depending on the internal structure of the nuclei and the properties of adjacent nuclei [19–23]. This diversity in decay processes and the potential to investigate them via proton emission correlation measurements have garnered significant interest and serve as crucial testing grounds for both nuclear physics and quantum theory.

Investigations beyond the proton dripline have revealed nuclei that are unbound with respect to new decay channels, including multi-proton emitters. This highlights the significance of such exotic decay modes as the precursor decay energy increases. Notable examples include nuclei that emit three protons ($3p$), such as ^{7}B [24], ^{17}Na [25], ^{31}K [26], and ^{13}F [27], as well as ground-state emitters of four protons ($4p$), like ^{8}C [28] and ^{18}Mg [29], and a five-proton ($5p$) emitter, ^{9}N [30]. Although the decay characteristics of many of these systems have not been investigated, analyses show that their decay may proceed in multiple steps, shedding excess protons through sequential $1p$ or $2p$ emission. ^{18}Mg, which has been recently discovered [29], decays via sequential $2p$–$2p$ emission of two pp pairs. Therefore, studies investigating whether the first-step $2p$ decay of ^{18}Mg resembles that of other $2p$ emitters and how the inner structure impacts this process are required.

Addressing the complexities of these phenomena requires sophisticated theoretical frameworks; however, comprehensive models that can simultaneously address the nuances of $2p$ and multi-proton emissions are still under development. Various approaches [31–34]have been employed, including the configuration interaction and density functional methods for structure analysis [35–40], and few-body methods for probing asymptotic proton correlations [41–45]. Innovations such as the shell model embedded in the continuum and the Gamow shell model integrate continuum effects into the configuration interaction framework, whereas hybrid methods leverage spectroscopic factors and few-body partial decay widths. Although the spectra and isospin-symmetry breaking between ^{18}Mg and mirror symmetry ^{18}C have been extensively investigated [46–49], the properties of the ^{18}Mg-^{18}C pair, especially the structures and time-dependent nucleon–nucleon correlations, have not yet been elucidated. This study employed the Gamow coupled-channel (GCC) method, a three-body approach that incorporates continuum effects, to investigate the decay dynamics and asymptotic correlations of 2p emitters, with a particular focus on the first-step 2p emission of ^{18}Mg and the configurations of its valence protons.

The remainder of this paper is organized as follows. Section II describes the models and Hamiltonian. In particular, it presents the framework of the GCC method and time-dependent approach. The structural and decay properties of ^{18}Mg are discussed in Section III. Finally, the summary is presented in Section IV.

II. Theoretical Model

A. Gamow coupled-channel approach(GCC)

In this study, we used a GCC approach [50, 51], which is a three-body model describing ^{18}Mg in terms of two valence protons and a core (^{16}Ne). To describe the three-body asymptotic behavior, the coordinates of ^{18}Mg can be expressed in Jacobi (relative) coordinates:

$$\begin{aligned}
\boldsymbol{x} &= \sqrt{\mu_x}(\boldsymbol{r}_{i_1} - \boldsymbol{r}_{i_2}), \\
\boldsymbol{y} &= \sqrt{\mu_y}\left(\frac{A_{i_1}\boldsymbol{r}_{i_1} + A_{i_2}\boldsymbol{r}_{i_2}}{A_{i_1} + A_{i_2}} - \boldsymbol{r}_{i_3}\right),
\end{aligned} \quad (1)$$

where $\boldsymbol{r}_i$ denotes the position vector of the ith cluster; $i_1 = p_1$, $i_2 = p_2$, and $i_3 = {}^{16}$Ne for the T-coordinate and $i_1 = {}^{16}$Ne, $i_2 = p_1$, and $i_3 = p_2$ for the Y-coordinate, as shown in Fig. 1(a,b). A_i is the mass number of the ith cluster. $\mu_x = \frac{A_{i_1}A_{i_2}}{A_{i_1}+A_{i_2}}$ and $\mu_y = \frac{(A_{i_1}+A_{i_2})A_{i_3}}{A_{i_1}+A_{i_2}+A_{i_3}}$ are the reduced masses associated with $\boldsymbol{x}$ and $\boldsymbol{y}$, respectively. These parameters can be used to describe the hyperradius $\rho = \sqrt{x^2 + y^2}$, which is transformation-invariant among different sets of Jacobi coordinates.

As the experimental measurements are performed in the momentum space, the relative momentum is defined as follows:

$$\begin{aligned}
\boldsymbol{k}_x &= \mu_x\left(\frac{\boldsymbol{k}_{i_1}}{A_{i_1}} - \frac{\boldsymbol{k}_{i_2}}{A_{i_2}}\right), \\
\boldsymbol{k}_y &= \mu_y\left(\frac{\boldsymbol{k}_{i_1} + \boldsymbol{k}_{i_2}}{A_{i_1} + A_{i_2}} - \frac{\boldsymbol{k}_{i_3}}{A_{i_3}}\right),
\end{aligned} \quad (2)$$

where $\boldsymbol{k}_i$ denotes the linear momentum of the ith cluster; θ_k and θ'_k are the opening angles of $(\boldsymbol{k}_x, \boldsymbol{k}_y)$ in the Jacobi-T and Jacobi-Y coordinates, respectively, as shown in Fig. 1(c), respectively. $E_{pp} = \frac{\hbar^2 k_x^2}{2\mu_x}$ represents the kinetic energy of the relative motion of the two emitted protons, and $E_{\text{core}-p}$ signifies that of the ^{16}Ne-p pair.

The total wave function in the Jacobi coordinates of the mother nucleus, which couples with the $p--p$ pair and ^{16}Ne, can be expressed as

$$\Psi^{J\pi} = \sum[\Phi^{J_p\pi_p} \otimes \phi^{J_c\pi_c}]^{J\pi}, \quad (3)$$

where $\phi^{J_c\pi_c}$ denotes the wave function of the core ^{16}Ne, and $\Phi^{J_p\pi_p}$ represents the wave function of the valence nucleons, which can be expressed as

$$\Phi^{J_p\pi_p} = \rho^{-5/2} \sum_{\gamma n K} C^{J_p\pi M}_{\gamma n K} \mathcal{B}^{J_p\pi}_{\gamma n}(\rho) \mathcal{Y}^{J_p M}_{\gamma K}(\Omega), \quad (4)$$

where $\mathcal{Y}^{J_p M}_{\gamma K}(\Omega)$ reprsents the hyperspherical harmonic of the hyper-angle. The hyperradial part is expanded in the Berggren ensemble, a complete basis in the complex-momentum plane including bound, decaying, and scattering states [50, 52, 53]. K is the hyperspherical quantum number, and $\gamma = \{s_1, s_2, S_{12}, S, \ell_x, \ell_y, L, J_p, J_c\}$ contains the other numbers. Using the Berggren basis, the inner and asymptotic
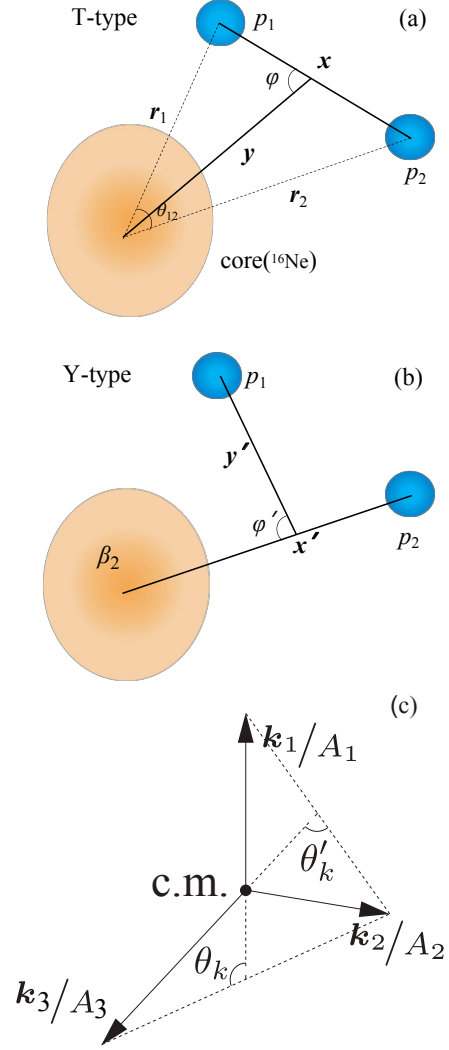

Fig. 1. Schematic of three-body ^{16}Ne + p +p system in Jacobi-T (a) and Jacobi-Y (b) coordinates. Momentum scheme (c) of three-body system.

regions of the Schrödinger equation can be addressed on the same footing, providing a natural connection between the nuclear structure and decay aspects of the problem.

The ^{16}Ne + p + p Hamiltonian of GCC can be expressed as

$$\hat{H} = \sum_{i=c,p_1,p_2} \frac{\hat{\boldsymbol{p}}_i^2}{2m_i} + \sum_{i>j=1}^{3} V_{ij}(\boldsymbol{r}_{ij}) + \hat{H}_c - \hat{T}_{\text{c.m.}}, \quad (5)$$

where $\hat{\boldsymbol{p}}_i^2/(2m_i)$ represents the kinetic operators of each particle, $V_{ij}(\boldsymbol{r}_{ij})$ denotes the interaction between clusters i and j, $\hat{H}_c$ is the core Hamiltonian given by the excitation energies of the core, and $\hat{T}_{\text{c.m.}}$ denotes the center-of-mass term. In Jacobi coordinates, the center of mass is automatically eliminated. In this study, the proton-core interaction V_{pc}, including the central, spin–orbit, and Coulomb terms, is approximated by a Woods–Saxon (WS) average potential[54–57].

To address the antisymmetrization between core and valence protons, a supersymmetric transformation method [58–

60]was employed. This method introduces an auxiliary repulsive "Pauli core" in the original core-p interaction to eliminate Pauli-forbidden states.

Consequently, the acquired eigenstate possesses a complex energy denoted by $\tilde{E} = E - i\Gamma/2$, where Γ represents the decay width. To elucidate the dynamics and asymptotic correlations inherent in the $2p$ decay, the wave function $\Psi^{J\pi}_{\mathrm{GCC}}$, derived within the complex framework, should be decomposed into real-momentum scattering states by applying the Fourier—Bessel series expansion. This approach is instrumental in reinstating the Hermitian characteristics of the Hamiltonian matrix and ensuring the conservation of total density. The initial wave packet, $\Psi^{J\pi}_{\mathrm{TD}}(t = 0)$, thus generated, can evolve over extended durations and distances within a time-dependent (TD) framework, as shown in Refs. [61, 62].

B. Hamiltonian and parameters

Magnesium isotopes often exhibit significant deformation. However, due to the lack of definitive experimental data on their deformation, the deformation factor is adopted from their mirror nucleus, ^{18}C, which exhibits a quadrupole deformation, β_2, of approximately 0.3, as reported in [63]. The ground and 2^+ states of the deformed core were considered through non-adiabatic coupling with the valence nucleons, and the corresponding energies were obtained from experimental data [63]. A previous study [38] reported significant mirror symmetry breaking in the ^{16}Ne-^{16}C mirror pair due to different configurations [64, 65]. However, the excitation energies of their first 2^+ states are remarkably similar, with ^{16}Ne at 1.77(0) MeV and ^{16}C at 1.76(6) MeV. Consequently, the breaking of mirror symmetry within the current framework cannot easily be described.

In a three-body system (^{16}Ne + p + p), the interaction between the two protons is described by the finite-range Minnesota force, adhering to the original parameters specified in Ref. [66]. This interaction is further supplemented by a two-body Coulomb force applied to protons. The core-proton (core $- p$) effective interaction was modeled using a WS potential (with a spin–orbit term) and one-body Coulomb interaction. The parameters of the WS potential, except for the potential depth V_0 and– the spin–orbit strength $V_{\mathrm{s.o.}}$, were retained as default values, as detailed in Ref. [67]. The spin–orbit strength was set to 24 MeV. Additionally, the depth V_0 was finely adjusted to accurately replicate the experimental ground state decay energy, $Q_{2p}(0^+\mathrm{g.s.}) = 3.44$ MeV, and the energy of the first 2^+ state, $E_x(2^+_1) = 1.84$ MeV, of ^{18}Mg, as discussed in Ref. [29].

The three-body configurations in Jacobi coordinates are labeled by quantum numbers (K, ℓ_x, ℓ_y, S), where ℓ_x represents the orbital angular momentum of the proton (neutron) pair with respect to their center of mass, ℓ_y is the orbital angular momentum of the pair with respect to the core, and S denotes the total intrinsic spin of the emitted nucleons. Three-body calculations were performed in the model space defined by $\max(\ell_x, \ell_y) \leqslant 8$ with a maximal hyperspherical quantum number $K_{\max} = 20$. For the hyperradial part, we used the Berggren basis for the $K \leqslant 3$ channels and the harmonic os-

cillator basis with an oscillator length of 1.75 fm and N_{max} = 20 for the remaining channels. For the GCC calculation of the initial state, the complex momentum contour defining the Berggren basis is given by the path $k = 0 \rightarrow 0.3 - 0.1i \rightarrow 0.4 - 0.05i \rightarrow 0.5 - 0.03i \rightarrow 0.8 \rightarrow 1.2 \rightarrow 2 \rightarrow 4 \rightarrow 6$ (all in fm^{-1}). For time-dependent evolution, the inner part (< 15 fm) of the initial state was expanded and propagated with a real-momentum contour, which followed $k = 0 \rightarrow 0.1 \rightarrow 0.13 \rightarrow 0.15 \rightarrow 0.16 \rightarrow 0.17 \rightarrow 0.185 \rightarrow 0.2 \rightarrow 0.225 \rightarrow 0.24 \rightarrow 0.25 \rightarrow 0.65 \rightarrow 0.8 \rightarrow 1.2 \rightarrow 2 \rightarrow 4 \rightarrow 6 \rightarrow 8$ (all in fm^{-1}). Each segment was discretized into 30 scattering states. In practice, interactions within a sphere of radius 250 fm were considered. However, because the wave function is defined in the momentum space and evolves from a highly localized initial wave packet, this cutoff has no practical effect on the investigated physical observables.

III. Results and Discussions

A. Structure information of ^{18}Mg and ^{18}C

A highly proton-rich nucleus, ^{18}Mg, located far from the β-stability line, has been recently identified as a $4p$ emitter [29]. The $4p$ decay proceeds through a two-step $2p$ decay via the intermediate ground state of ^{16}Ne. To elucidate the internal structure of ^{18}Mg and its influence on decay properties, we begin by examining the spectrum and valence-proton configurations of ^{18}Mg and comparing them with its mirror partner, ^{18}C. The mirror pair, due to isospin symmetry, typically exhibits similar properties across many aspects. However, Coulomb interactions introduce discrepancies in their thresholds. Consequently, ^{18}Mg is particle-unbound, with a $2p$ separation energy of $S_{2p}(^{18}\mathrm{Mg}) = -3.44$ MeV, whereas ^{18}C is bound to a $2n$ separation energy of $S_{2n}(^{18}\mathrm{C}) = 4.92$ MeV, as determined experimentally.

The calculated spectra of ^{18}Mg and ^{18}C align qualitatively, if not quantitatively, with the experimental data. Specifically, the excitation energy of the first $2+$ state is slightly underestimated for ^{18}Mg. Meanwhile, although only one 2^+ state is observed experimentally, our calculation predicts two low-lying 2^+ states, similar to the situation in its mirror system ^{18}C. The ground state of ^{18}Mg is less unbound than those of ^{17}Na and ^{16}Ne. Considering the large decay width of ^{17}Na, the ground state of ^{18}Mg might have a "democratic" decay mode, which exhibits open $1p$ and $2p$ decay channels. This suggests potential competition between $1p$ and $2p$ decay modes during the decay process of ^{18}Mg. To determine the primary decay mechanism, we used a time-dependent approach to analyze the corresponding decay dynamics (see the discussion below).

However, due to the Coulomb interaction, ^{18}Mg is less bound than its mirror partner, indicating a greater continuum effect. As presented in Table 1, the sd-shell effect significantly influences the ground-state configuration of valence neutrons in ^{18}C, favoring the configurations $(K, \ell_x, \ell_y, S) = (4,0,0,0)$ and $(4,1,1,1)$, which primarily correspond to the d orbital. However, for ^{18}Mg in its ground state, the $(0,0,0,0)$ configuration (s orbital) is essential. This is because ^{18}Mg

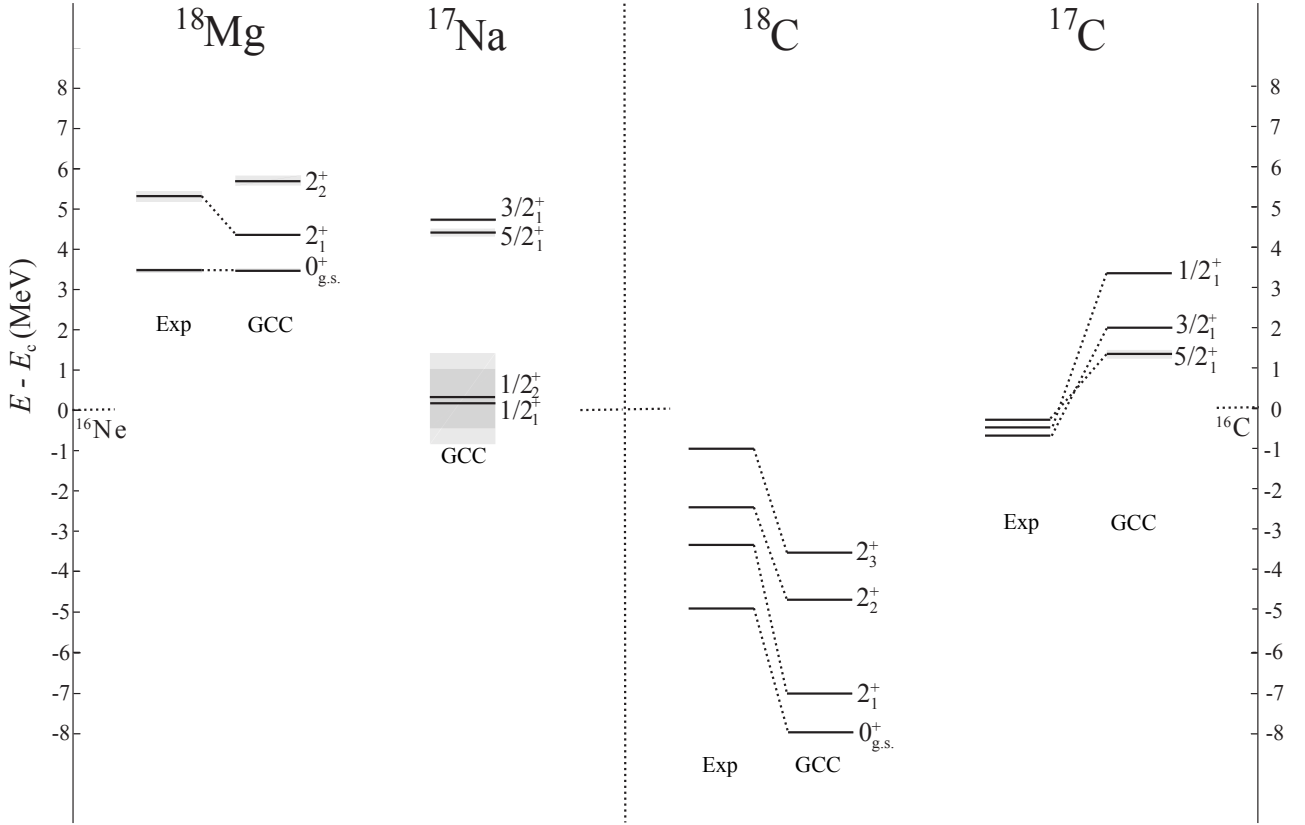Fig. 2. The calculated spectra and decay widths (shaded areas) of ^{18}Mg-^{18}C pair and related neighboring nuclei ^{17}Na and ^{17}C. Experimental data were obtained from Refs. [29, 63].

TABLE 1. Predicted configurations (K, ℓ_x, ℓ_y, S) and the corresponding weights of ^{18}Mg and ^{18}C.

J^π	(K, ℓ_x, ℓ_y, S)	
	^{18}Mg	^{18}C
$0^+_{g.s.}$	34.86% (4,0,0,0)	39.68% (4,0,0,0)
	19.36% (4,1,1,1)	25.82% (4,1,1,1)
	18.00% (0,0,0,0)	6.83% (4,0,2,0)
2^+_1	13.36% (4,0,2,0)	17.28% (4,1,1,1)
	11.61% (2,0,2,0)	14.10% (4,0,0,0)
	8.29% (4,0,0,0)	13.59% (4,0,2,0)
2^+_2	25.51% (4,2,2,0)	25.57% (4,1,1,1)
	16.41% (4,1,1,1)	13.67% (4,2,2,0)
	4.39% (8,4,4,0)	11.06% (4,0,0,0)
2^+_3		23.39% (4,0,0,0)
		15.51% (4,1,1,1)
		9.15% (2,0,2,0)

better interacts with the continuum than ^{18}C, rendering the s-wave component favorable owing to its reduced centrifugal barrier. This effect is also observed in the spectral analysis of the odd-A neighboring nuclei ^{17}Na and ^{17}C, where the $1/2^+$ state in ^{17}Na, despite being unbound, benefits from additional binding from the continuum, establishing it as the ground state. Conversely, the state sequence in the mirror nucleus ^{17}C exhibits a different arrangement. This discrepancy in the energy levels between particle-bound and unbound mir-

ror systems is a characteristic of the Thomas–Ehrman shift [68–70].

Regarding the 2^+ states, although the pure s-wave component is forbidden by the angular momentum selection rule, the influence of the continuum is still noticeable, causing the configuration $(K, \ell_x, \ell_y, S) = (2,0,2,0)$ to be pronounced in ^{18}Mg, where the K quantum number represents the three-body centrifugal barrier. This leads to similar excitation energies for the 2^+ states of ^{18}C and ^{18}Mg, although different continuum effects are involved in these systems.

The internal structures of ^{18}C and ^{18}Mg also exhibit moderate mirror symmetry breaking, which is similar to that of the ^{16}C-^{16}Ne mirror pair. As illustrated by the density distributions of the valence nucleons shown in Fig. 3, the ground state of ^{18}Mg exhibits a more expansive distribution than that of ^{18}C, although both nuclei possess di-nucleon, cigar-like structures, and a small triangular component internally. This discrepancy is due to the significant s-wave component and unbound nature of ^{18}Mg. Meanwhile, the internal structures of the 2^+_1 states appear analogous to the ground for both ^{18}Mg and ^{18}C because most components are built upon the excited state of the daughter nuclei.

The properties of the related nucleus, ^{17}Na, have also attracted considerable attention due to limited experimental data availability. Energy spectra have been calculated in several studies to predict the decay scheme of ^{17}Na [71, 72]. In addition, to assess the effect of deformation on structural characteristics and decay properties, we computed the energy
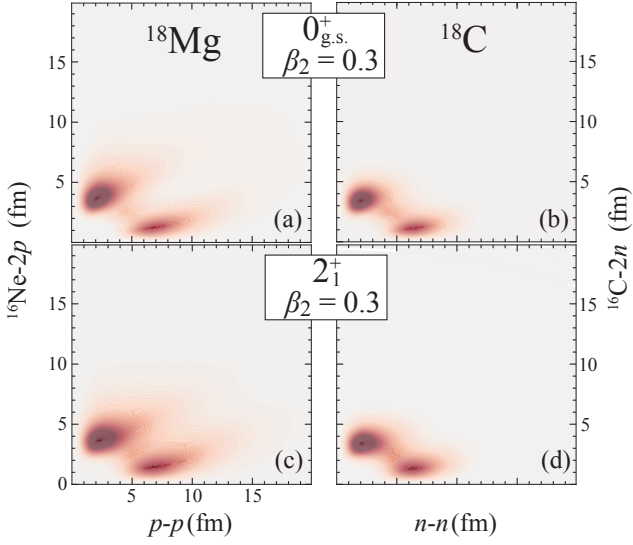
Fig. 3. $2p$ (left) and $2n$ (right) density distributions in Jacobi-T coordinate predicted for the ground and first excited states of ^{18}Mg (left) and ^{18}C (right), respectively.

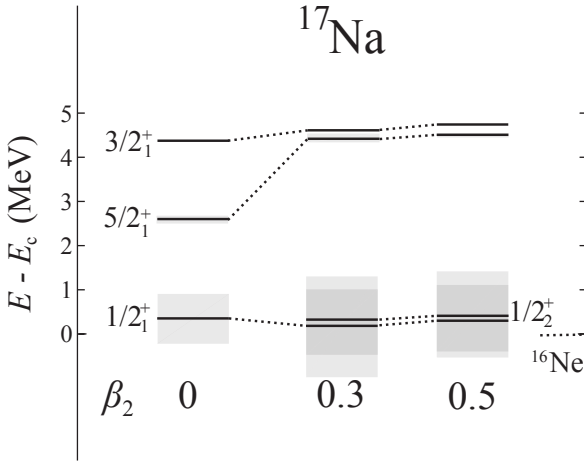Fig. 4. Calculated spectrum of ^{17}Na as a function of quadrupole deformation β_2.

spectrum of ^{17}Na and the $2p$ density distributions of the ^{18}Mg ground state as functions of the quadrupole deformation parameter β_2 (refer to Figs. 4 and 5). The analysis of the spectral evolution of ^{17}Na reveals a gap between the s and d orbitals with increasing deformation. This gap is also observed as the $(K, \ell_x, \ell_y, S) = (4,0,0,0)$ and $(4,1,1,1)$ configurations decreases from a spherical shape to a prolate deformation in the ground state of ^{18}Mg. Consequently, this results in a change in the primary structure of ^{18}Mg, as shown in Fig. 5. Notably, considerable deformation ($\beta_2 = 0.5$) represents uniform density distribution.

B. Decay properties of ^{18}Mg

The internal configurations and spectroscopic details of ^{18}Mg and its adjacent nuclei have been reported previously.
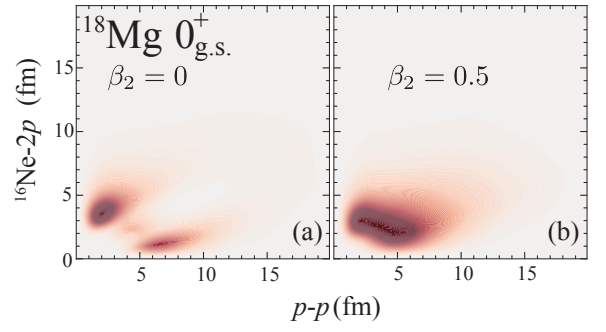

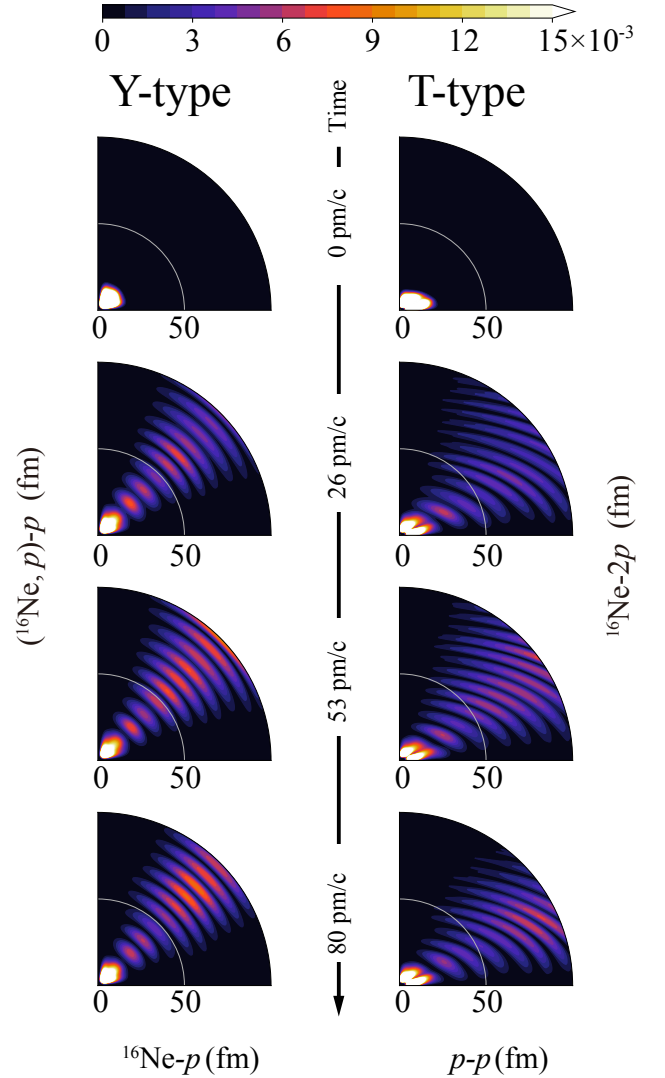Fig. 5. Ground-state density distributions of ^{18}Mg with (a) spherical and (b) $\beta_2 = 0.5$ deformations.

Fig. 6. Time evolution of the ground state of ^{18}Mg with a quadrupole deformation $\beta_2 = 0.3$. Density distributions of two emitted protons are shown in Jacobi-Y (left) and -T (right) coordinates for four different time slices.
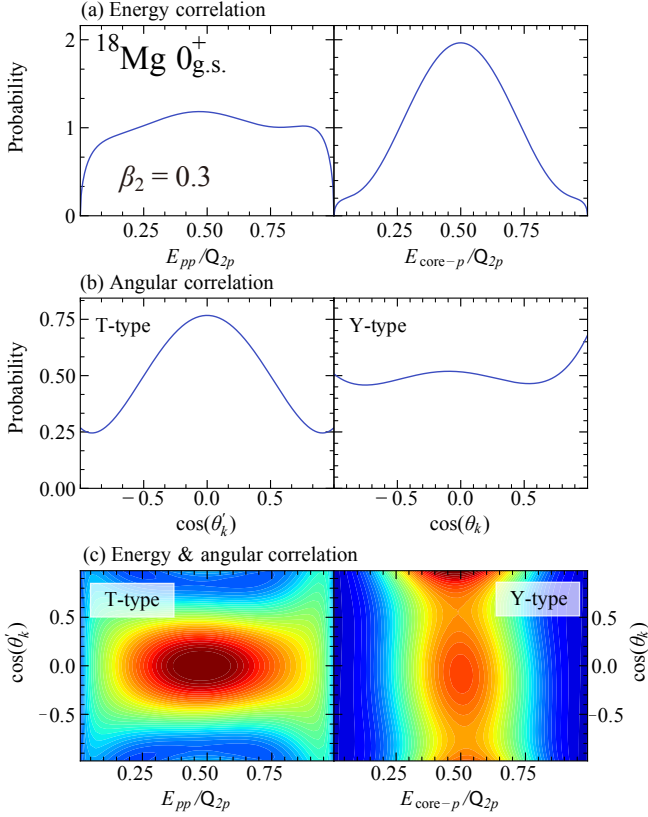
Fig. 7. Asymptotic energy (a), angular (b), and two-dimensional correlations of two emitted protons from the ground state of ^{18}Mg with β_2 deformation of 0.3 in Jacobi-T (left) and -Y (right) coordinates, respectively. Q_{2p} is the total decay energy.

Fig. 8. Similar to Fig. 7 but for the β_2 deformation of 0.5.

An intriguing aspect to further examine is the influence of these properties on the decay dynamics and mechanisms. For this purpose, we employed a time-dependent framework to evolve the initial wave function across extensive spatial and temporal scales, as shown in Fig. 6.

Initially ($t = 0$), most of the ^{18}Mg ground-state wave function was confined within the nuclear boundary, forming the discussed diproton and cigar-like structures. However, the density evolution within the Jacobi-T coordinate reveals the merging of these structures during the tunneling phase; a dynamic distinct from the decay behavior observed in the p-shell nucleus ^{6}Be [61] but similar to that of the sd-shell nucleus ^{12}O [73]. This similarity is attributed to the substantial s-wave component and relatively large decay energy/width characteristic of the ^{18}Mg ground state. Concurrently, in the decay process, the distance between ^{16}Ne and a proton remains similar to the increasing separation in the $(^{16}$Ne,$p)$-p configuration, as observed in the density evolution depicted in the Jacobi-Y coordinate shown in Fig. 6. This observation suggests that, despite the energetic feasibility of single-proton decay for the ^{18}Mg ground state, simultaneous two-proton emission is the most probable decay mode.

The correlations between protons emitted from the ground state of ^{18}Mg are shown in Fig. 7. Given the notably wide decay widths associated with light–mass systems, the energy or angular distributions canno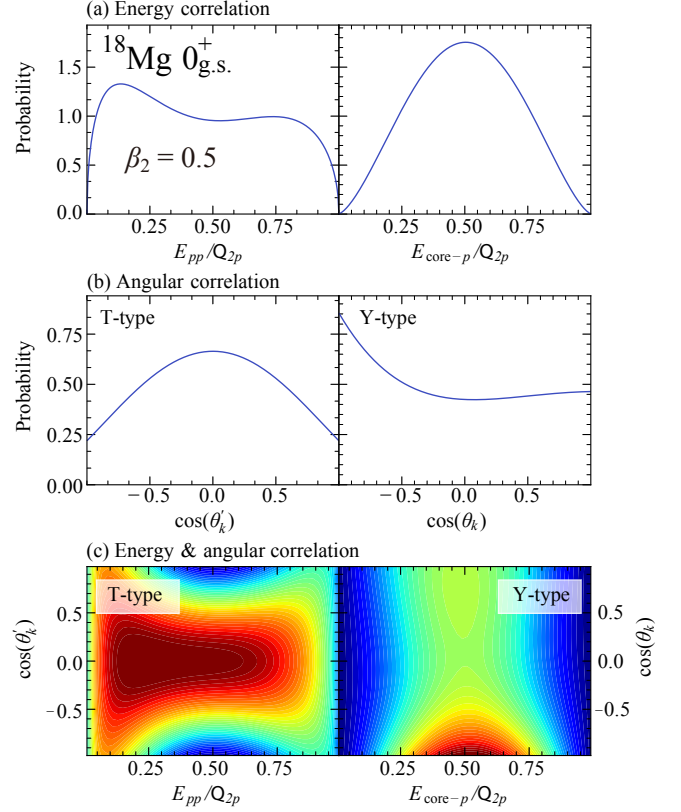t easily reveal distinct patterns that could differentiate between decay mechanisms. Specifically, for ^{18}Mg, the energy correlation of the T-type is almost uniform, which is attributed to the substantial s-wave component within the ground-state wave function, as previously discussed. Meanwhile, the Y-type energy correlation attains a noticeable peak around E_{core-p}/Q_{2p}, further supporting the likelihood of a simultaneous $2p$ emission, rather than a sequential decay process.

Furthermore, we investigated the effect of deformation on the asymptotic correlations of ^{18}Mg, as shown in Figs. 7 and 8. When the quadrupole deformation β_2 changes from 0 to 0.3, the asymptotic correlation is slightly affected. However, the T-type energy correlation and Y-type angular correlation are significantly changed for $\beta_2 = 0.5$. This is in accordance with the change in the internal structure/configuration as deformation increases. In particular, enhanced peaks are observed in the small E_{pp} and large θ_k regions (see Fig. 8), which might indicate a diproton emission, although the density of the valence proton inside the nucleus is uniformly distributed for $\beta_2 = 0.5$ (see Fig. 5). Given that nucleon–nucleon correlation can be directly measured, further experimental investigations are required.

IV. Summary

In this study, we investigated the structure and $2p$ decay mechanism of ^{18}Mg using a three-body Gamow-coupled-channel model and compared it with its mirror partner, ^{18}C.

Our analysis revealed that although both systems exhibited di-nucleon and cigarlike structures in their valence nucleon configurations, moderate mirror symmetry breaking occurred in the density distributions and spectroscopy due to the Thomas–Ehrman effect. The influence of the continuum on the ground state of ^{18}Mg induced a significant s-wave component.

The structural characteristic of ^{18}Mg led to widespread distribution of the nucleon–nucleon correlation within the asymptotic region, similar to the behavior of other $2p$ emitters in the light–mass region. Furthermore, decay dynamics analysis showed that ^{18}Mg underwent simultaneous $2p$ emission in the initial decay step, despite the energetically permitted $1p$ decay channel.

In addition, we investigated the effects of deformation on structural and decay properties. Results showed that deformation could alter the level gap and introduce the mixing of different components, consequently affecting primary structures. Therefore, further experiments are required to determine the inner structure and corresponding nucleon–nucleon correlation.

[1] V.I. Goldansky, On neutron-deficient isotopes of light nuclei and the phenomena of proton and two-proton radioactivity. Nucl. Phys. **19**, 482–495 (1960). doi:10.1016/0029-5582(60)90258-3

[2] V.I. Goldansky, 2-proton radioactivity. Nucl. Phys. **27**, 648–664 (1961). doi:10.1016/0029-5582(61)90309-1

[3] J. Giovinazzo, B. Blank, M. Chartier et al., Two-proton radioactivity of ^{45}Fe. Phys. Rev. Lett. **89**, 102501 (2002). doi:10.1103/PhysRevLett.89.102501

[4] M. Pfützner, E. Badura, C Bingham et al., First evidence for the two-proton decay of ^{45}Fe. Eur. Phys. J. A **14**, 279–285 (2002). doi:10.1140/epja/i2002-10033-9

[5] B. Blank, M. Płoszajczak, Two-proton radioactivity. Rep. Prog. Phys. **71**, 046301 (2008). doi:10.1088/0034-4885/71/4/046301

[6] L.V. Grigorenko, Theoretical study of two-proton radioactivity. status, predictions, and applications. Phys. Part. Nucl. **40**, 674–714 (2009). doi:10.1134/S1063779609050049

[7] L. Zhou, D.Q. Fang, S.M. Wang et al., Recent progress in two-proton radioactivity. Nucl. Sci. Tech. **33**, 105 (2022). doi:10.1007/s41365-022-01091-1

[8] M. Pfützner, I. Mukha, S.M. Wang, Two-proton emission and related phenomena. Prog. Part. Nucl. Phys. **123**, 104050 (2023). doi:10.1016/j.ppnp.2023.104050

[9] Z.Y. Yuan, D. Bai, Z. Wang et al., Research on two-proton radioactivity in density-dependent cluster model. Sci. China-Phys. Mech. Astron. **66**, 222012 (2023). doi:10.1007/s11433-022-1994-8

[10] F. Catara, A. Insolia, E. Maglione et al., Relation between pairing correlations and two-particle space correlations. Phys. Rev. C **29**, 1091–1094 (1984). doi:10.1103/PhysRevC.29.1091

[11] N. Pillet, N. Sandulescu, P. Schuck, Generic strong coupling behavior of Cooper pairs on the surface of superfluid nuclei. Phys. Rev. C **76**, 024310 (2007). doi:10.1103/PhysRevC.76.024310

[12] K. Hagino, H. Sagawa, Pairing correlations in nuclei on the neutron-drip line. Phys. Rev. C **72**, 044321 (2005). doi:10.1103/PhysRevC.72.044321

[13] K. Hagino, H. Sagawa, J. Carbonell et al., Coexistence of BCS-and BEC-like pair structures in halo nuclei. Phys. Rev. Lett. **99**, 022506 (2007). doi:10.1103/PhysRevLett.99.022506

[14] Y.Y. Chu, Z.Z. Ren, Properties of proton-rich nuclei in a three-body model. Eur. Phys. J. A **37**, 361–366 (2008). doi:10.1140/epja/i2008-10626-2

[15] L.V. Grigorenko, T.D. Wiser, K. Miernik et al., Complete correlation studies of two-proton decays: ^{6}Be and ^{45}Fe. Phys. Lett. B **677**, 30–35 (2009). doi:10.1016/j.physletb.2009.04.085

[16] C.J. Lin, X.X. Xu, H.M. Jia et al., Experimental study of two-proton correlated emission from ^{29}S excited states. Phys. Rev. C **80**, 014310 (2009). doi:10.1103/PhysRevC.80.014310

[17] C.J. Lin, X.X. Xu, H.M. Jia et al., Experimental study of the two-proton correlated emission from the excited states of ^{17,18}Ne and ^{28,29}S. Nucl. Phys. A **834**, 450c–453c (2010), the 10th International Conference on Nucleus-Nucleus Collisions (NN2009). doi:10.1016/j.nuclphysa.2010.01.061

[18] K. Hagino, H. Sagawa, Correlated two-neutron emission in the decay of the unbound nucleus ^{26}O. Phys. Rev. C **89**, 014331 (2014). doi:10.1103/PhysRevC.89.014331

[19] M. Matsuo, Spatial structure of Cooper pairs in nuclei, in *Fifty Years of Nuclear BCS*, ed. by R.A. Broglia, V. Zelevinsky (World Scientific Publishing, Singapore, 2012), p. 61–72. doi:10.1142/9789814412490_0005

[20] I. Mukha, L.V. Grigorenko, X. Xu et al., Observation and spectroscopy of new proton-unbound isotopes ^{30}Ar and ^{29}Cl: An interplay of prompt two-proton and sequential decay. Phys. Rev. Lett. **115**, 202501 (2015). doi:10.1103/PhysRevLett.115.202501

[21] Y.G. Ma, D.Q. Fang, X.Y. Sun et al., Different mechanism of two-proton emission from proton-rich nuclei ^{23}Al and ^{22}Mg. Phys. Lett. B **743**, 306–309 (2015). doi:10.1016/j.physletb.2015.02.066

[22] K. Fossez, J. Rotureau, N. Michel et al., Continuum effects in neutron-drip-line oxygen isotopes. Phys. Rev. C **96**, 024308 (2017). doi:10.1103/PhysRevC.96.024308

[23] J. Casal, M. Gómez-Ramos, Opening angle and dineutron correlations in knockout reactions with borromean two-neutron halo nuclei. Phys. Rev. C **104**, 024618 (2021). doi:10.1103/PhysRevC.104.024618

[24] R.J. Charity, J.M. Elson, J. Manfredi et al., Isobaric multiplet mass equation for A=7 and 8. Phys. Rev. C **84**, 051308 (2011). doi:10.1103/PhysRevC.84.051308

[25] K.W. Brown, R.J. Charity, J.M. Elson et al., Proton-decaying states in light nuclei and the first observation of ^{17}Na. Phys. Rev. C **95**, 044326 (2017). doi:10.1103/PhysRevC.95.044326

[26] D. Kostyleva, I. Mukha, L. Acosta et al., Towards the limits of existence of nuclear structure: Observation and first spectroscopy of the isotope ^{31}K by measuring its three-proton decay. Phys. Rev. Lett. **123**, 092502 (2019). doi:10.1103/PhysRevLett.123.092502

[27] R.J. Charity, T.B. Webb, J.M. Elson et al., Observation of the exotic isotope ^{13}F located four neutrons beyond the proton drip line. Phys. Rev. Lett. **126**, 132501 (2021). doi:10.1103/PhysRevLett.126.132501

[28] R.J. Charity, J.M. Elson, J. Manfredi et al., $2p$-$2p$ decay of ^{8}C and isospin-allowed $2p$ decay of the isobaric-analog state in ^{8}B. Phys. Rev. C **82**, 041304 2010. doi:10.1103/PhysRevC.82.041304

[29] Y. Jin, C.Y. Niu, K.W. Brown et al., First observation of the four-proton unbound nucleus ^{18}Mg. Phys. Rev. Lett. **127**,

262502 (2021). doi:10.1103/PhysRevLett.127.262502

[30] R.J. Charity, J. Wylie, S.M. Wang et al., Strong evidence for ^{9}N and the limits of existence of atomic nuclei. Phys. Rev. Lett. **131**, 172501 (2023). doi:10.1103/PhysRevLett.131.172501

[31] Y. Suzuki, K. Ikeda, Cluster-orbital shell model and its application to the He isotopes. Phys. Rev. C **38**, 410–413 (1988). doi:10.1103/PhysRevC.38.410

[32] D. Baye, P. Descouvemont, N.K. Timofeyuk, Matter densities of ^{8}B and ^{8}Li in a microscopic cluster model and the proton-halo problem of ^{8}B. Nucl. Phys. A **577**, 624–640 (1994). doi:10.1016/0375-9474(94)90936-9

[33] N. Michel, W. Nazarewicz, M. Płoszajczak et al., Gamow shell model description of neutron-rich nuclei. Phys. Rev. Lett. **89**, 042502 (2002). doi:10.1103/PhysRevLett.89.042502

[34] F.C. Barker, R-matrix formulas for three-body decay widths. Phys. Rev. C **68**, 054602 (2003). doi:10.1103/PhysRevC.68.054602

[35] P. Descouvemont, D. Baye, The R-matrix theory. Rep. Progr. Phys. **73**, 036301 (2010). doi:10.1088/0034-4885/73/3/036301

[36] K. Hagino, H. Sagawa, Decay dynamics of the unbound ^{25}O and ^{26}O nuclei. Phys. Rev. C **93**, 034330 (2016). doi:10.1103/PhysRevC.93.034330

[37] T. Oishi, M. Kortelainen, A. Pastore, Dependence of two-proton radioactivity on nuclear pairing models. Phys. Rev. C **96**, 044327 (2017). doi:10.1103/PhysRevC.96.044327

[38] L.V. Grigorenko, I.G. Mukha, I.J. Thompson et al., Two-proton widths of ^{12}O, ^{16}Ne, and three-body mechanism of thomas-ehrman shift. Phys. Rev. Lett. **88**, 042502 (2002). doi:10.1103/PhysRevLett.88.042502

[39] L.V. Grigorenko, T.D. Wiser, K. Mercurio et al., Three-body decay of ^{6}Be. Phys. Rev. C **80**, 034602 (2009). doi:10.1103/PhysRevC.80.034602

[40] T.A. Golubkova, X.D. Xu, L.V. Grigorenko et al., Transition from direct to sequential two-proton decay in s–d shell nuclei. Phys. Lett. B **762**, 263–270 (2016). doi:10.1016/j.physletb.2016.09.034

[41] H.T. Zhang, D. Bai, Z. Wang et al., Complex scaled nonlocalized cluster model for ^{8}Be. Phys. Rev. C **105**, 054317 (2022). doi:10.1103/PhysRevC.105.054317

[42] D.M. Zhang, L.J. Qi, D.X. Zhu et al., Systematic study on the proton radioactivity of spherical proton emitters. Nucl. Sci. Tech. **34**, 55 (2023). doi:10.1007/s41365-023-01201-7

[43] D.X. Zhu, Y.Y. Xu, H.M. Liu et al., Two-proton radioactivity of the excited state within the gamowlike and modified gamow-like models. Nucl. Sci. Tech. **33**, 122 (2022). doi:10.1007/s41365-022-01116-9

[44] D.X. Zhu, Y.Y. Xu, L.J. Chu et al., Two-proton radioactivity from excited states of proton-rich nuclei within coulomb and proximity potential model. Nucl. Sci. Tech. **34**, 130 (2023). doi:10.1007/s41365-023-01268-2

[45] Z.Z. Zhang, C.X. Yuan, C. Qi et al., Extended R-matrix description of two-proton radioactivity. Phys. Lett. B **838**, 137740 (2023). doi:10.1016/j.physletb.2023.137740

[46] A. Yakhelef, N.K. Timofeyuk, J.S. Al-Khalili et al., Three-body spectrum of ^{18}C and its relevance to r-process nucleosynthesis. Few-Body Syst. **47**, 213–224 (2010). doi:10.1007/s00601-010-0086-8

[47] P. Voss, T. Baugher, D. Bazin et al., Excited-state transition-rate measurements in ^{18}C. Phys. Rev. C **86**, 011303 (2012). doi:10.1103/PhysRevC.86.011303

[48] Y. Kondo, T. Nakamura, Y. Satou et al., One-neutron removal reactions of ^{18}C and ^{19}C on a proton target. Phys. Rev. C **79**, 014602 (2009). doi:10.1103/PhysRevC.79.014602

[49] N. Michel, J.G. Li, F.R. Xu et al., Proton decays in ^{16}Ne and ^{18}Mg and isospin-symmetry breaking in carbon isotopes and isotones. Phys. Rev. C **103**, 044319 (2021). doi:10.1103/PhysRevC.103.044319

[50] S.M. Wang, N. Michel, W. Nazarewicz et al., Structure and decays of nuclear three-body systems: The Gamow coupled-channel method in Jacobi coordinates. Phys. Rev. C **96**, 044307 (2017). doi:10.1103/PhysRevC.96.044307

[51] S.M Wang, W. Nazarewicz, Puzzling two-proton decay of ^{67}Kr. Phys. Rev. Lett. **120**, 212502 (2018). doi:10.1103/PhysRevLett.120.212502

[52] L.V. Grigorenko, M.V. Zhukov, Two-proton radioactivity and three-body decay. II. Exploratory studies of lifetimes and correlations. Phys. Rev. C **68**, 054005 (2003). doi:10.1103/PhysRevC.68.054005

[53] T. Berggren, On the use of resonant states in eigenfunction expansions of scattering and reaction amplitudes. Nucl. Phys. A **109**, 265–287 (1968). doi:10.1016/0375-9474(68)90593-9

[54] K. Hagino, N. Rowley, A.T. Kruppa, A program for coupled-channel calculations with all order couplings for heavy-ion fusion reactions. Comput. Phys. Commun. **123**, 143–152 (1999). doi:10.1016/S0010-4655(99)00243-X

[55] K. Hagino, Role of dynamical particle-vibration coupling in reconciliation of the $d_{3/2}$ puzzle for spherical proton emitters. Phys. Rev. C **64**, 041304 (2001). doi:10.1103/PhysRevC.64.041304

[56] B. Barmore, A.T. Kruppa, W. Nazarewicz et al., Theoretical description of deformed proton emitters: Nonadiabatic coupled-channel method. Phys. Rev. C **62**, 054315 (2000). doi:10.1103/PhysRevC.62.054315

[57] A.T. Kruppa, W. Nazarewicz, Gamow and r-matrix approach to proton emitting nuclei. Phys. Rev. C **69**, 054311 (2004). doi:10.1103/PhysRevC.69.054311

[58] I.J. Thompson, B.V. Danilin, V.D. Efros et al., Pauli blocking in three-body models of halo nuclei. Phys. Rev. C **61**, 024318 (2000). doi:10.1103/PhysRevC.61.024318

[59] I.J. Thompson, F.M. Nunes, B.V. Danilin, FaCE: a tool for three body Faddeev calculations with core excitation. Comput. Phys. Commun. **161**, 87–107 (2004). doi:10.1016/j.cpc.2004.03.007

[60] P. Descouvemont, C. Daniel, D. Baye, Three-body systems with lagrange-mesh techniques in hyperspherical coordinates. Phys. Rev. C **67**, 044309 (2003). doi:10.1103/PhysRevC.67.044309

[61] S.M. Wang, W. Nazarewicz, Fermion pair dynamics in open quantum systems. Phys. Rev. Lett. **126**, 142501 (2021). doi:10.1103/PhysRevLett.126.142501

[62] S.M. Wang, W. Nazarewicz, A. Volya et al., Probing the nonexponential decay regime in open quantum systems. Phys. Rev. Res. **5**, 023183 (2023). doi:10.1103/PhysRevResearch.5.023183

[63] Evaluated Nuclear Structure Data File (ENSDF). http://www.nndc.bnl.gov/ensdf/

[64] N. Michel, J.G. Li, L.H. Ru et al., Calculation of the thomas-ehrman shift in ^{16}F and ^{15}O(p,p) cross sections within the gamow shell model. Phys. Rev. C **106**, L011301 (2022). doi:10.1103/PhysRevC.106.L011301

[65] J.G. Li, N. Michel, W Zuo et al., Resonances of A=4 T=1 isospin triplet states within the ab initio no-core gamow shell model. Phys. Rev. C **104**, 024319 (2021). doi:10.1103/PhysRevC.104.024319

[66] D.R. Thompson, M. Lemere, Y.C. Tang, Systematic investigation of scattering problems with the resonating-group method. Nucl. Phys. A **286**, 53–66 (1977). doi:10.1016/0375-9474(77)90007-0

[67] C.R. Bain, P.J. Woods, R. Coszach et al., Two proton emission induced via a resonance reaction. Phys. Lett. B **373**, 35–39

(1996). doi:10.1016/0370-2693(96)00109-8

[68] J.B. Ehrman, On the displacement of corresponding energy levels of C^{13} and N^{13}. Phys. Rev. **81**, 412–416 (1951). doi:10.1103/PhysRev.81.412

[69] R.G. Thomas, An analysis of the energy levels of the mirror nuclei, C^{13} and N^{13}. Phys. Rev. **88**, 1109–1125 (1952). doi:10.1103/PhysRev.88.1109

[70] S.M. Wang, W. Nazarewicz, R.J. Charity et al., Structure and decay of the extremely proton-rich nuclei $^{11,12}O$. Phys. Rev. C **99**, 054302 (2019). doi:10.1103/PhysRevC.99.054302

[71] N.K. Timofeyuk, P. Descouvemont, Narrow states in the three-proton emitter ^{17}Na. Phys. Rev. C **81**, 051301 (2010). doi:10.1103/PhysRevC.81.051301

[72] H.T. Fortune, R. Sherr, Coulomb energies in ^{16}Ne and low-lying levels of ^{17}Na. Phys. Rev. C **82**, 027310 (2010). doi:10.1103/PhysRevC.82.027310

[73] S.M. Wang, W. Nazarewicz, R.J. Charity et al., Nucleon–nucleon correlations in the extreme oxygen isotopes. J. Phys. G: Nucl. Part. Phys. **49**, 10LT02 (2022). doi:10.1088/1361-6471/ac888f